Supplemental Table 1

Clinical characteristics of MS patients and controls.

Cases	Gender	age	Clinical diagnosis	Lesion
MS389	F	55	Secondary progressive MS	Chronic active
MS402	M	46	Secondary progressive MS	Chronic active
MS403	F	54	Secondary progressive MS	Chronic acute
MS404	F	55	Secondary progressive MS	Acute active
MS406	M	62	Secondary progressive MS	Acute active
MS407	F	44	Secondary progressive MS	Acute active
MS408	M	39	Secondary progressive MS	Acute active
MS410	F	47	Secondary progressive MS	Acute active
MS411	M	61	Secondary progressive MS	Acute active
MS416	M	55	Secondary progressive MS	Acute active
MS418	M	56	Secondary progressive MS	Acute acute
C075	M	88	urinary infection, COPD	Control
C073	M	71	Liver Cancer	Control
C072	M	77	Pneumonia, ischemic bowel	Control
C036	M	68	Myocardial infarcts	Control
C044	F	67	Acute arrhythmia	Control
C067	F	67	Metastatic ovarian cancer	Control
C054	M	66	pancreatic cancer	Control

Supplemental Fig. 1

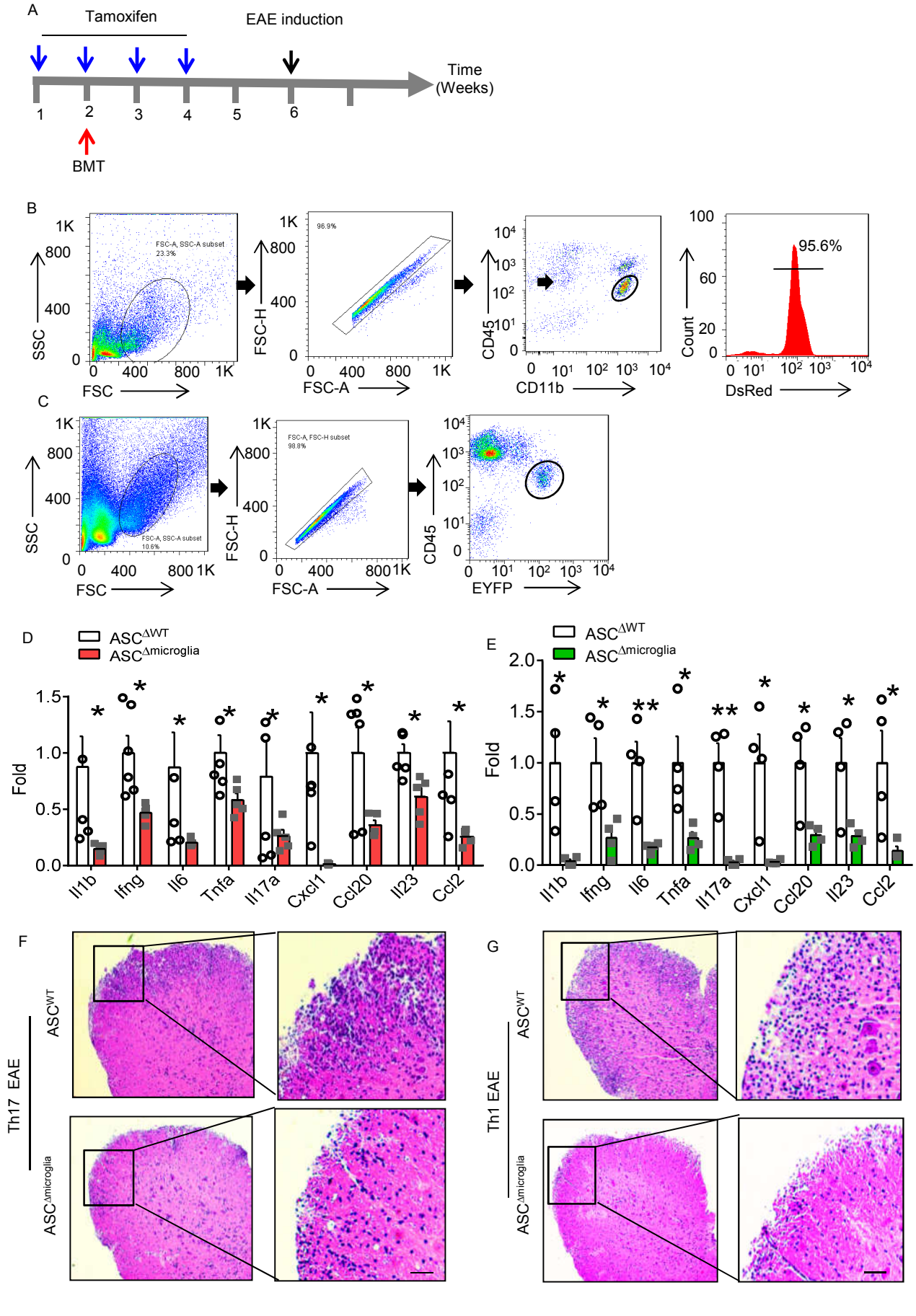

Supplemental Fig. 2

Casp8 Peptide Sequences detected by Mass Spectrometry

1. DCFICCILSHGDK
2. FLCLDYIPHK
3. TMLAENNLETLK
4. WDLLVNFLDCNR

Supplemental Fig. 3

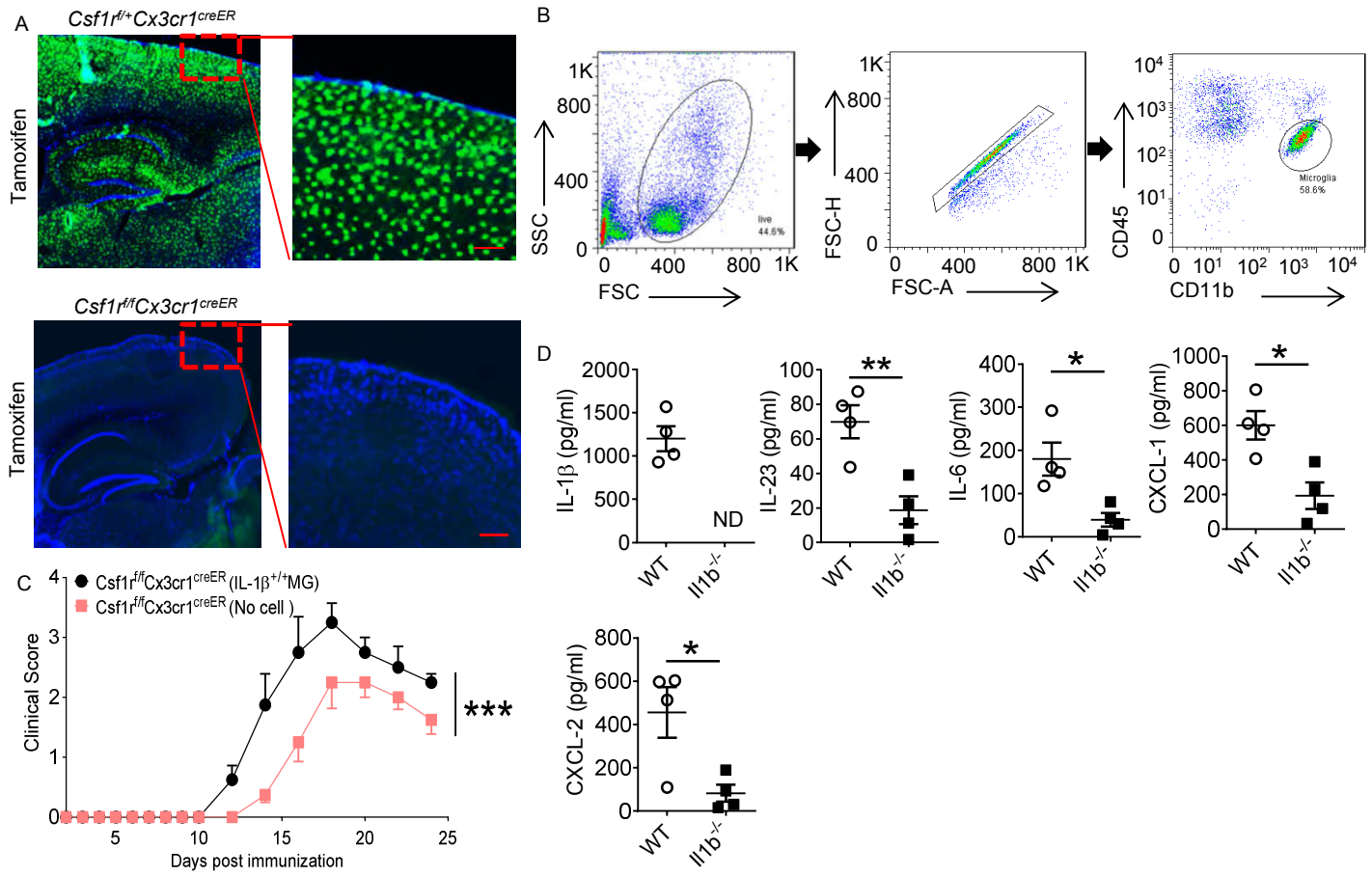

Supplemental Figure Legends

Supplemental Figure 1. Microglia intrinsic ASC promote both Th17 and Th1 induced EAE. Analysis of results for WT→*Asc*$^{f/+}$*Cx3cr1*$^{Cre\text{-}ER}$ (ASC$^{\Delta WT}$) and WT→*Asc*$^{f/f}$*Cx3cr1*$^{Cre\text{-}ER}$ (ASC$^{\Delta microglia}$) bone marrow chimera mice in EAE disease. (**A**) Schematic diagram of tamoxifen treatment, bone marrow transplantation and EAE induction. (**B**) Analysis of efficiency of Cre recombinase in microglia of *Asc*$^{f/+}$*Cx3cr1*$^{Cre\text{-}ER}$*Rosa26-stop-DsRed* mice. (**C**) Gating strategy of EYFP^{+} microglia during EAE disease. (**D and E**) Inflammatory gene expression in the lumbar spinal cords as assessed at the peak of disease induce by Th17 (D, N=6/group) or Th1 (E, N=5/group) transfer. (**F and G**) H&E staining of lumbar spinal cords harvested at the peak of disease. Scale Bar, 100 μm. Data are representative of two independent experiments; Mean ± SEM. *P < 0.05, * *P < 0.01 (unpaired two-tailed *t*-test).

Supplemental Figure 2. IRAKM physically interacts with caspase-8. (**A**) Mass spectrometry analysis of IRAKM-associated proteins after immunoprecipitation via anti-IRAKM beads from cell lysates and four matched peptide sequences that correspond to caspase-8 were detected.

Supplemental Figure 3. Characterization of IL-1b KO microglia. (**A**) Tamoxifen was administered to *Csf1r*$^{f/f}$*Cx3cr1*^{Cre} mice at 5 mg/mouse by i.p for consecutive four weeks (1 time/week) followed by DAPI staining and microscope analysis of microglia cells deletion. EYFP indicates microglia cells and Blue indicates nuclear. Scale Bar, 400 μm. (**B**) Gating strategy of microglia from WT and *Il1b*$^{-/-}$ donor mice**.** (**C**) *Csf1r*$^{f/f}$ *Cx3cr1*^{cre} mice were treated with tamoxifen and transferred with or without wild-type microglia after the fourth tamoxifen injection. N=6/group. (**D**) ELISA analysis of inflammatory cytokines and chemokines in the supernatant of primary microglia isolated from EAE brain at peak disease. N=4/group. Data are representative of two independent experiments; Mean ± SEM.